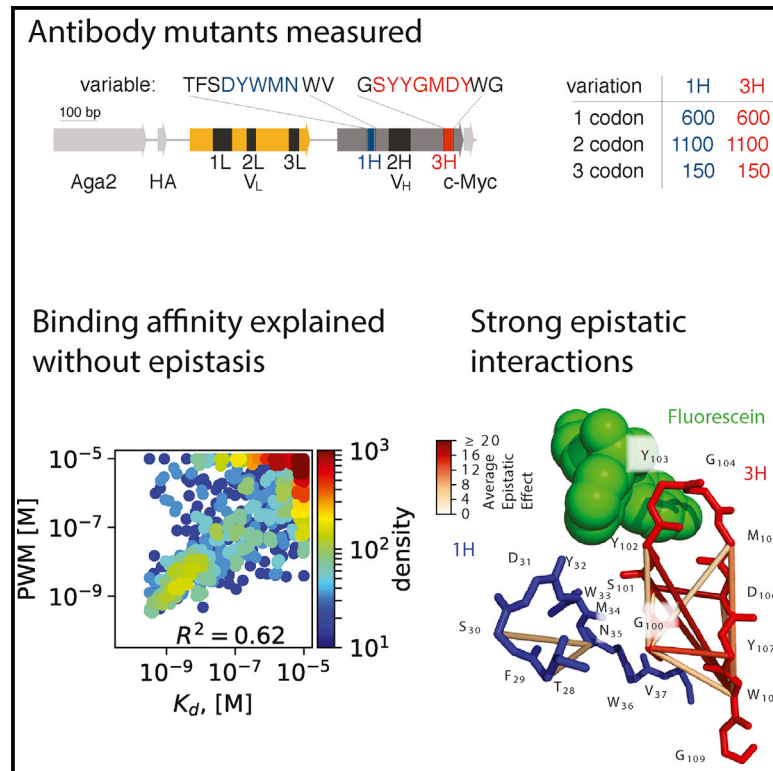# Epistasis in a Fitness Landscape Defined by Antibody-Antigen Binding Free Energy

Graphical Abstract

Authors

Rhys M. Adams, Justin B. Kinney,
Aleksandra M. Walczak, Thierry Mora

Correspondence

awalczak@lpt.ens.fr (A.M.W.),
tmora@lps.ens.fr (T.M.)

In Brief

Epistasis plays a major role in molecular evolution, shaping fitness landscapes into valleys and ridges and hindering or facilitating adaptation. Here, we analyze epistasis in massively parallel measurements of antibody affinity to an antigenic target. We find pervasive epistasis, including beneficial ones, suggesting a more complex landscape than previously appreciated.

Highlights

- Epistatic effects are extracted from massive measurements of binding energies

- Variability in binding is 62% due to additive effects and 25%–35% due to epistasis

- Up to 4% of double mutants have sign epistasis

- Simulations suggest that epistasis may expand paths of affinity maturation

Brief Report

Epistasis in a Fitness Landscape Defined by Antibody-Antigen Binding Free Energy

Rhys M. Adams,[1,2] Justin B. Kinney,[2] Aleksandra M. Walczak,[1,*] and Thierry Mora[3,4,*]

[1]CNRS, Laboratoire de Physique Théorique, UPMC (Sorbonne University), and École Normale Supérieure (PSL), 24 rue Lhomond, Paris 75005, France
[2]Simons Center for Quantitative Biology, Cold Spring Harbor Laboratory, 1 Bungtown Rd., Cold Spring Harbor, NY 11724, USA
[3]CNRS, Laboratoire de Physique Statistique, UPMC (Sorbonne University), Paris-Diderot University, and École Normale Supérieure (PSL), 24, rue Lhomond, Paris 75005, France
[4]Lead Contact
*Correspondence: awalczak@lpt.ens.fr (A.M.W.), tmora@lps.ens.fr (T.M.)
https://doi.org/10.1016/j.cels.2018.12.004

SUMMARY

Epistasis is the phenomenon by which the effect of a mutation depends on its genetic background. While it is usually defined in terms of organismal fitness, for single proteins, it must reflect physical interactions among residues. Here, we systematically extract the specific contribution pairwise epistasis makes to the physical affinity of antibody-antigen binding relevant to affinity maturation, a process of accelerated Darwinian evolution. We find that, among competing definitions of affinity, the binding free energy is the most appropriate to describe epistasis. We show that epistasis is pervasive, accounting for 25%–35% of variability, of which a large fraction is beneficial. This work suggests that epistasis both constrains, through negative epistasis, and enlarges, through positive epistasis, the set of possible evolutionary paths that can produce high-affinity sequences during repeated rounds of mutation and selection.

INTRODUCTION

To ensure a reliable response and neutralize foreign pathogens, the adaptive immune system relies on affinity maturation. In this process, antibody receptors expressed by B cells undergo an accelerated Darwinian evolution through random mutations and selection for affinity against foreign epitopes (Cobey and Wilson, 2015). Mature antibodies can accumulate up to 20% hyper-mutations from their germline sequence (Marcou et al., 2018), leading to up to a 10,000-fold improvement in binding affinity (Eisen and Siskind, 1964). Affinity maturation also produces broadly neutralizing antibodies that target conserved regions of the pathogen, of particular importance for vaccine design against fast evolving viruses (Corti and Lanzavecchia, 2013). Despite extensive experimental and theoretical work, the key determinants of antibody specificity and evolvability are still poorly understood, mainly because the sequence-to-affinity relationship is difficult to measure comprehensively or to predict computationally (Esmaielbeiki et al., 2016).

A major confounding factor in characterizing the sequence dependence of any protein function, including affinity, is the pervasiveness of epistasis, the phenomenon by which different mutations interact with each other (Phillips, 2008). Theory (Carter et al., 2005; Good and Desai, 2015; Paixão and Barton, 2016) and genomic data (Breen et al., 2012) suggest that inter- and intragenic epistasis play a major role in molecular evolution by constraining the set of accessible evolutionary trajectories toward adapted phenotypes (Weinreich et al., 2006; Poelwijk et al., 2007; Gong et al., 2013; Anderson et al., 2015; Podgornaia and Laub, 2015), enhancing evolvability through stabilization of mutations (Bloom et al., 2006, 2010), or slowing down adaptation by the law of diminishing returns (Chou et al., 2011; Kryazhimskiy et al., 2014). Evidence for epistasis in antibody affinity includes direct observations of co-operativity between mutations (Midelfort et al., 2004; Koenig et al., 2015), the dependence of mutational effects on sequence background (Boyer et al., 2016), and statistical co-variation of residues in large sequence datasets (Mora et al., 2010; Asti et al., 2016).

Intragenic epistasis has mostly been studied either by measuring the fitness of all possible mutational intermediates between two variants (Weinreich et al., 2006; Schenk et al., 2013; Szendro et al., 2013; de Visser and Krug, 2014) or by comparing the effect of mutations in different backgrounds (Jacquier et al., 2013; Bank et al., 2015; Boyer et al., 2016). Many such studies rely on a particular measure of fitness rather than a well-defined physical phenotype. Deep mutational scans (DMS) (Fowler and Fields, 2014; Sarkisyan et al., 2016) can comprehensively map out the epistatic landscape of many genetic variants (Araya et al., 2012; Olson et al., 2014; Podgornaia and Laub, 2015). However, most DMS methods do not measure the biophysical quantity of interest directly (Vodnik et al., 2011), introducing both non-linearities and noise that could be misinterpreted as epistasis.

Here, we analyze the detailed epistatic landscape of an antibody's binding free energy, which we define as the logarithm of the Tite-Seq measurement of the dissociation constant, to its cognate antigen (the 4-4-20 antibody fragment against fluorescein), using data previously obtained by Tite-Seq, a recently introduced DMS variant that accurately measures protein binding affinity in physical units of molarity (Adams et al., 2016). By comparing to a simple additive model of mutations on the
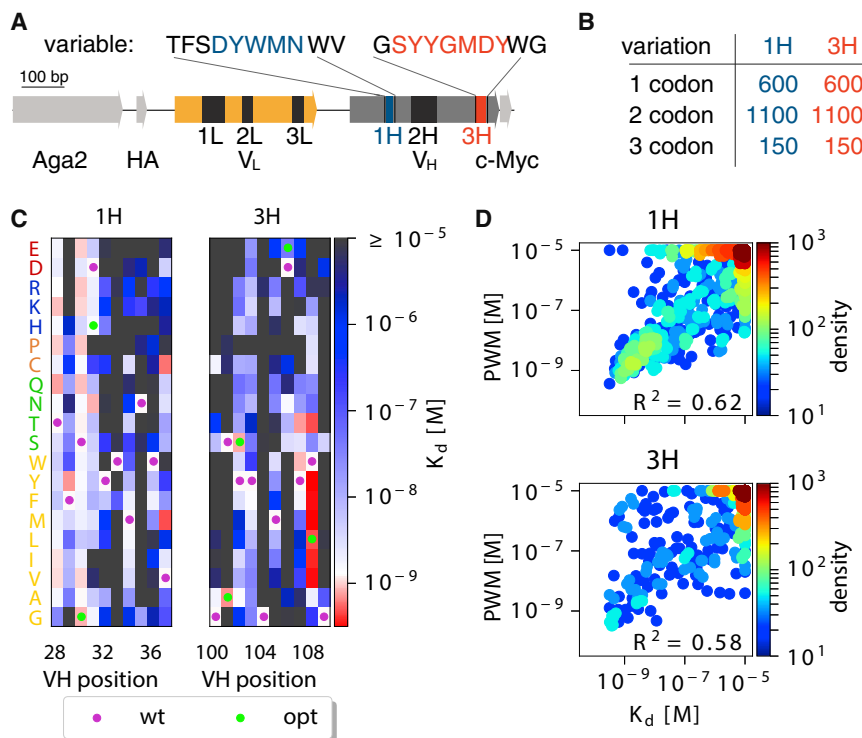
Figure 1. Additive Model of Binding Affinity

(A) 4-4-20 scFv antibody sequence. Six complementarity determining regions (CDR: 1L, 2L, 3L, 1H, 2H, and 3H) are particularly important for antibody binding affinity. A library of antibody sequences with mutations in 10 amino acid regions around the CDR1H and CDR3H domains were expressed using yeast display.

(B) Using Tite-Seq, the binding constants K_d of all 600 single codon mutants, 1,100 random double codon mutants, and 150 random triple codon mutants, were measured.

(C) The K_d of single mutants for 1H and 3H domains were used to create position weight matrices (PWMs) to predict the affinity of double and triple mutants. K_d measurements were restricted to the reliable measurements interval of $10^{-9.5}$ to 10^{-5} M. WT sequences are marked with purple dots, optimized 4M5.3 (RRID: Addgene_41844) mutations are marked in green dots.

(D) Comparison between the PWM prediction and the measurement of K_d on double and triple mutants. PWM predictions outside of our reliable readout interval ($10^{-9.5}$ to 10^{-5} M) were evaluated at the interval boundaries. The PWMs explained a significant portion of the variance, as quantified by the explained variance R^2 (p < 10^{-61} for CDR1H, p < 10^{-48} for CDR3H, F test for reduction in variance due to PWM). PWMs trained from the binding free energy, $F = \ln(K_d/c_0)$, outperformed PWM trained from K_d (Figure S3) as well as models without boundaries (Figure S4).

binding free energy, and carefully controlling for measurement noise and nonlinearities, we find that epistasis significantly contributes to the antibody's affinity. This epistasis is not uniformly distributed but instead favors certain residue pairs across the protein. We use our results to analyze how epistasis both constrains and enlarges the set of possible evolutionary paths leading to high-affinity sequences.

RESULTS

Position Weight Matrix Model of Affinity

We analyzed data from (Adams et al., 2016) (https://github.com/jbkinney/16_titeseq), where Tite-Seq was applied to measure the binding affinities of variants of the 4-4-20 fluorescein-binding scFv antibody, henceforth called "wild-type." Libraries were generated by introducing mutations to either the CDR1H or CDR3H domains restricted to 10 amino acid stretches called 1H and 3H (Figure 1A). All single amino acid mutants, 1,100 random double amino acid mutants, and 150 triple amino acid mutants were generated in multiple synonymous variants and measured (Figure 1B). Using a combination of yeast display and high-throughput sequencing at various antigen concentrations, Tite-Seq yielded the binding dissociation constant K_d (in M or mol/L) of each variant with the fluorescein antigen.

We first tried to predict the K_d of double and triple mutants from single mutant measurements. Mutations are expected to act on the binding free energy in an approximately additive way (Wells, 1990; Olson et al., 2014). One may thus write the free energy of binding, $F = \ln(K_d/c_0)$ (defined up to constant in

units of $k_B T$), as a sum over mutations in the mutagenized region, $\mathbf{s} = (s_1, \ldots, s_l)$:

$$F(\mathbf{s}) \approx F_{PWM}(\mathbf{s}) = F_{WT} + \sum_{i=1}^{l} h_i(s_i), \qquad \text{(Equation 1)}$$

where F_{WT} is the wild-type sequence energy, and $h_i s_i$ is the effect of a mutation at position i to residue s_i. The elements of the position-weight matrix (PWM) $h_i(s_i)$ are obtained from the K_d of single mutants shown in Figure 1C. Since Tite-Seq measurements are limited to values of K_d ranging from $10^{-9.5}$ to 10^{-5}, for consistency PWM predictions outside this range were set to the boundary values. The PWM was a fair predictor of double and triple mutants (Figure 1D), accounting for 62% (p < 10^{-61}, F test) of the variance for 1H mutants and 58% (p < 10^{-48}, F test) of the variance of 3H mutants. In contrast, a simple model based on BLOSUM62 scores (Łuksza et al., 2017) achieved far lower R^2 scores of 22 and 3% for the CDR-1H and 3H domains, respectively Figure S1).

The unexplained variance missed by the PWM model may have four origins: convolution with expression, nonlinear effects, measurement noise, and epistasis. Tite-seq was developed specifically to separate the measurement K_d and expression. From Pearson's correlation between expression and log(K_d), we find that expression explains 6% and 12% of the R^2 for CDR1H and CDR3H, respectively (Figure S2). Furthermore, the residual from the PWM prediction, $F - F_{PWM}$, had almost no correlation with expression (R^2 < 0.1% for 1H, R^2 < 0.2% for 3H, Figure S2). Log transformed expression values yielded similar but smaller contributions. The second "non-linear

effects" case corresponds to the hypothesis of additivity not being valid for $F = \ln(K_d/c_0)$ but for some other non-linear transformations of F. Such a non-linearity, also called "scale," can lead to spurious epistasis (Fisher, 1918; Phillips, 2008). We first checked that additivity did not apply to the untransformed dissociation constant, K_d: a PWM model learned from K_d instead of F could only explain 34% of the variance of all 1H and 3H multiple mutants, down from 62% when learning from F (Figure S3). Refitting Tite-seq values with no boundary constraints yielded much worse PWM models, largely attributable to poor estimates of poorly binding antibodies (Figure S4). We then looked for the nonlinear transformation $E(F)$ that would give the PWM model with the best predictive power (STAR Methods; Figure S5). This optimization yielded only a modest improvement to 65% of the explained variance. In addition, the optimal function E was very close to the logarithm ($R^2 = 97\%$, Figure S6). Since nonlinear effects do not play a significant role, henceforth, we only consider the PWM model defined on the free energy.

Epistasis Affects Affinity

To identify epistasis, we estimated the difference between the measured binding free energies of double and triple mutants, $F(s)$, and the PWM prediction, $F_{PWM}(s)$ (Figure 2A). However, these small differences can be confounded by measurement noise (Figure S7), which can be mistaken for epistasis. To control for this noise, we defined Z-scores between two estimates of the free energy, F_a and F_b, as $Z = (F_a - F_b)/\sqrt{\sigma_a^2 + \sigma_b^2}$, where σ_a^2 and σ_b^2 are their estimates of uncertainty. Uncertainty was either measured as variance from replicate measurements and synonymous mutations or as the sum of variances from additive PWM contributions depending on context. We first computed Z-scores between independent estimates of the same free energy using synonymous variants (Z_{error}, STAR Methods). Excluding mutants at the reliable readout boundary ($10^{-9.5}$ M $\leq K_d \leq 10^{-5}$ M), we found that the distribution of Z_{error} was normal with variance ≈ 1 (Figure 2B, orange line), as expected from Gaussian measurement noise. A comparison between Tite-seq measurements and clones K_d measured from flow cytometry was also approximately normal with variance ≈ 1 (Figure S8), meaning that Tite-Seq introduced no systematic errors in addition to those estimated from replicates.

We then estimated the effect of epistasis by calculating Z-scores (Z_{epi}) from the difference between the PWM prediction, F_{PWM} (Equation 1), and the measured F. The resulting distributions of Z-scores (Figure 2A, blue and red lines) had much larger variances than expected from measurement noise (standard deviation 1.76 for 1H and 3.18 for 3H), indicating strong epistasis. These epistatic effects were on average slightly beneficial (positive Z): 18% of double mutants inside the reliable readout boundaries ($10^{-9.5}$ M $\leq K_d \leq 10^{-5}$ M) showed significant beneficial epistasis ($Z_{epi} > 1.64$, corresponding to p < 0.05 in a one-sided Z test), and 12% significant deleterious epistasis ($Z_{epi} < -1.64$). Comparing the variance of Z_{epi} with that of Z_{error} gives a large fraction of the unexplained variance that is attributable to epistasis, $1 - Var(Z_{error})/Var(Z_{epi}) = 60\%$ for 1H and 88% for 3H. While clones at the reliable readout boundaries under-estimated measurement error, their inclusion yielded

more extreme results (Figure S9). PWMs trained from optimal transformations had almost no effect on epistasis estimates (Figure S10).

To determine whether certain positions along the sequence concentrated epistatic effects, we computed the mean squared Z-score for all double mutations at each pair of positions (excluding median boundary values), revealing a complex and heterogeneous landscape of epistasis (Figures 2C and S11 for the epistasis magnitude superimposed on the wild-type's crystal structure). CDR3H, which interacts directly with the antigen, is observed to have more epistatically interacting sites than CDR1H. Interestingly, the three most epistatic pairs in 3H—between positions 101, 106, and 108—are mutated in the previously described super-optimized 4M5.3 antibody (Boder et al., 2000) (mutations shown in green in Figure 1B), consistent with previous suggestions that positions 101 and 106 interact together and with position 108 via hydrogen bonds (Midelfort et al., 2004; Adams et al., 2016). Epistasis is usually expected between residues that are in contact in the protein structure (Romero et al., 2013; Morcos et al., 2011; McLaughlin et al., 2012; Zhang et al., 2013; Melamed et al., 2013), as for instance between positions 101 and 106. However, the mean squared Z-score is only weakly correlated with residue distance (r = −0.13, p = 0.22 for 1H, r = −0.27, p = 0.022 for 3H, Figure S12). Additionally, while distance to antigen has been shown to predict how strongly mutations affect binding affinity (Brenke et al., 2012; Kepler et al., 2014), we did not detect a strong relationship between epistatic contributions and distance to antigen (r = −0.24, p = 0.511 for 1H, r = 0.19, p = 0.603 for 3H, Figure S12F). This may be due in part to this study's mutated region being too close to the antigen to detect an association: 12 out of the 20 mutated residues are within 10 Å of the antigen and all 20 are within 16 Å.

We next looked for evidence of "sign epistasis," where one mutation reverses the sign of the effect of another mutation (Figure 2A). Sign epistasis can constrain evolution by blocking paths to fit sequences (Weinreich et al., 2006; Poelwijk et al., 2011; Weinreich et al., 2005). We defined a Z-score for a single mutation A quantifying the beneficial effect of that mutation relative to the noise, $Z_A = (F_{WT} - F_A)/\sigma_A$, where F_{WT} and F_A are the wild-type and mutant-free energies and σ is the measurement error estimated as before. Since we are only interested in the sign of the effect, we kept single mutants at the reliable readout boundary. An equivalent Z-score was defined for a mutation A in the background of an existing mutation B: $Z_{A|B} = (F_B - F_{AB})/\sqrt{\sigma_A^2 + \sigma_{AB}^2}$, where F_{AB} is the free energy of the double mutant AB. Significant sign epistasis was defined by $Z_{A|B}Z_A < 0$ and $|Z_{A|B}|, |Z_A| > 1.64$, and reciprocal sign epistasis by the additional symmetric condition $A \leftrightarrow B$.

With a 5% false discovery rate (Benjamin Hochberg procedure), we found 52 significant sign epistasis examples. These are listed in S1_table_sign_epistasis.csv and summarized in Tables S1 and S2. Deleterious sign epistasis was exceptional, with 3 instances in 1H and 6 in 3H. These cases, as well as the four most significant cases of beneficial sign epistasis are depicted in Figure S13. These mutants represent evolutionary trajectories blocked due to the poor binding affinity of their single mutations. Among cases where both single mutations were deleterious, we found 4% (p < 10^{-15}, binomial test) of mutants in 1H

CellPress
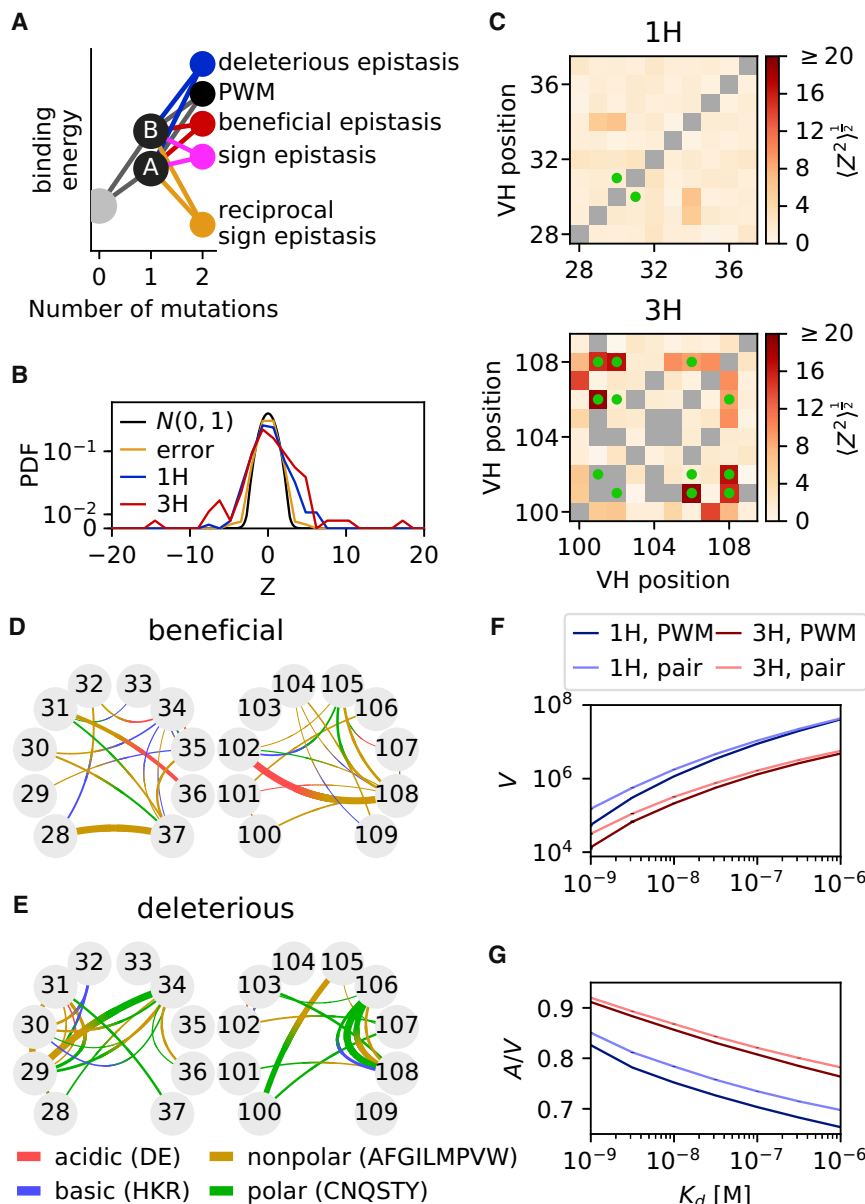
Figure 2. Quantification of Epistasis

(A) Epistasis is defined as deviation from the PWM model, which assumes an additive effect of single mutations on the binding free energy $F = \ln(K_d/c_0)$ expressed in units of k_BT. Deleterious epistasis occurs when the measured energy exceeds the PWM prediction. Beneficial epistasis occurs when the energy is less than the PWM prediction. Sign and reciprocal sign epistasis examples are shown for a beneficial interaction.

(B) Distribution of Z-scores, defined as the normalized deviation from the PWM prediction, $Z_{\mathrm{epi}} = (F_{\mathrm{PWM}} - F)/\sqrt{\sigma^2 + \sigma^2_{\mathrm{PWM}}}$, where σ^2 and σ^2_{PWM} are the estimated errors on F and F_{PWM}. K_d at boundaries are removed. Positive Z-scores indicate epistasis increased affinity. The Z-score standard deviation was much higher than expected from measurement errors (Z_{error}) for CDR1H (1.78, p $< 10^{-16}$, Levene's test) and CDR3H (3.18, p $< 10^{-48}$), meaning that the discrepancy between the PWM and measurement is mainly due to true epistasis.

(C) Standard Z-score deviation for each pair of positions along the sequence. This deviation is higher at pairs of positions mutated in the super-optimized 4M5.3 antibody (green dots) in 3H (p = 0.005, Mann-Whitney), but not in 1H (p = 0.36).

(D and E) A model of biochemical epistatic interactions between polar, nonpolar, acidic, and basic residues was fitted to the data using LASSO regularization and tested by cross-validation, yielding (D) 34 beneficial, and (E) 32 deleterious interaction terms. Line width denotes interaction strength.

(F) Number V of amino-acid sequences of the 1H (blue) and 3H (red) regions with dissociation constant below K_d, as estimated by the PWM model (dark color) or the epistatic model (light color). Epistasis enlarges the number of variants with good affinity for both 1H and 3H.

(G) Mutational flux A (defined as the average number of random mutation events from all possible sequences to cause the dissociation constant to cross K_d), normalized by V, showing that epistasis also increases the accessibility of the region of good binders in sequence space. Differences between the PWM and epistatic models were robust to errors in the estimate of the interaction parameters (p $< 10^{-5}$, Jackknife analysis).

and 0.8% (p $< 10^{-7}$, binomial test) in 3H with significant beneficial epistasis versus 0.06% expected by chance (the null expectation, which takes into account the constraint that $Z_A + Z_{B|A} = Z_B + Z_{A|B}$, is defined in the STAR Methods); 1% (p $< 10^{-15}$, binomial test) were reciprocal in 1H, and 0.4% (p $< 10^{-10}$, Binomial test) in 3H, versus 0.01% expected by chance. To evaluate how these epistatic interactions may affect affinity maturation, we estimated how often "viable" double mutants were separated from the wild-type by nonviable single mutants, where viability is defined by $K_d < 10^{-6}$ M (Batista and Neuberger, 1998; Foote and Eisen, 1995; Roost et al., 1995), forming possible roadblocks to affinity maturation. This strong instance of "rescue" epistasis occurred in roughly half of the mutants with beneficial sign epistasis (Tables S1 and S2).

Modeling Epistasis and Its Impact on Affinity Maturation

To integrate the observed epistatic interactions into a predictive model of affinity, we introduced a model of binding free energy as the following:

$$F(\mathbf{s}) \approx F_{\mathrm{pairwise}}(\mathbf{s}) = F_{\mathrm{PWM}}(\mathbf{s}) + \sum_{i<j} J_{ij}(s_i, s_j), \qquad \text{(Equation 2)}$$

where J_{ij} is the interaction strength between residues at positions i and j. To avoid overfitting and allow for independent validation (in the absence of a sufficient number of triple mutants), we grouped residues into 4 biochemical categories (Voet and Voet, 2011) (polar, nonpolar, acidic, and basic; STAR Methods) and let the entries of J only depend on that category.

We trained the model on the 1,208 1H or 1,216 3H double and triple mutants, using a Lasso penalty to control for overfitting. The optimal penalty was set by 10-fold cross-validation, i.e. by maximizing the explained variance of a subset comprising 1/10 of the mutants by using a model trained on the remaining 9/10, averaged over the 10 subsets (Figure S14A; STAR Methods). Interacting pairs with posterior probabilities >0.95 as determined by Bayesian Lasso (Park and Casella, 2008) are shown in Figures 2D and 2E.

Out of the 360 possible terms, 52 1H and 45 3H interaction terms were identified by this method. Although these interactions, whose number is limited by the number of measured variants, only modestly improved the explained variance relative to the PWM in all multiple mutants (from 62% to 64% for 1H and from 58% to 60% for 3H), it substantially improved the affinity prediction of the mutants with significant epistasis (R^2 from 27% to 50% in 1H and from 13% to 44% in 3H, Figures S14B and S14C). In contrast, a null linear regression model based on the Miyazawa-Jernigen matrix had negligible improvement on R^2 (Figure S15) (George et al., 2017) Notably, two mutations of the super-optimized 4M5.3 antibody are predicted by the model to have epistatic interactions, a slightly deleterious effect between A_{101} and L_{108}, and a strongly beneficial one between S_{102} and L_{108}. While these results show some generalizability of biochemical properties, the corresponding model only accounts for a small fraction of the variance explainable by epistasis. A more sophisticated approach may be warranted for fully predicting epistatic contributions.

Next we used our models to estimate the diversity, or "degeneracy," of antibodies with good binding affinity. Specifically, we evaluated the degeneracy volume V of high-affinity sequences as the number of sequences with $K_d < B$, using either the PWM (Equation 1) or pairwise (Equation 2) models, and using a combination of exhaustive and Monte-Carlo sampling (STAR Methods). Compared to the coarse-grained pairwise model trained previously, the interaction strength J was learned directly for each residue pair, without grouping by biochemical category and with no Lasso penalty. The volume of 1H mutants was larger than that of 3H mutants (Figure 2F), in agreement with the fact that CDR3H plays a more important role in binding affinity. Epistasis increased the recognition volume for both domains, consistent with the previous observation that epistatic effects are, on average, more beneficial than deleterious. To explore the diversity of evolutionary paths leading to recognition, we computed the neutral mutational flux A in and out of the high-affinity region as the probability that a random mutation in a high-affinity sequence ($K_d < B$) causes loss of recognition ($K_d > B$), summed over all high-affinity sequences (STAR Methods). Again, our models show increased mutational flux due to epistasis, even after normalizing by volume, A/V (Figure 2G). The effect is small, but only reflects the impact of epistasis from the limited, randomly chosen set of double mutations that we measured, which comprises only ~7% of all possible double mutations of a 10 amino acid sequence (1,058 for CDR1H, and 1,066 for CDR3H, out of 16,245). We speculate that differences in flux arising from all epistatic interactions may be up to 15-fold stronger. Adding explicit selection to the mutational model would also affect the results but would require that additional assumptions are made about how binding affinity and selection are linked.

The neutral mutational flux analysis allows for comparisons that do not depend on such an explicit model of selection.

We checked that these differences were robust to sampling noise and overfitting by performing a jackknife analysis (p < 10^{-5}) for the difference in A and V between the PWM and pairwise models, STAR Methods, and verified that similar conclusions were obtained based on the optimized nonlinear transformation (Figure S16).

DISCUSSION

By analyzing massively parallel affinity measurements obtained by Tite-Seq, we obtained a detailed picture of epistasis in a well-defined physical phenotype—the binding free energy of an antibody to an antigen. Here, we define the free energy as the logarithm of the dissociation constant as measured by Tite-Seq and the yeast display assay. While our analysis of epistasis strictly applies to that measured phenotype and not directly to the free energy, these two quantities are believed to be equivalent (VanAntwerp and Wittrup, 2000). We showed that antibody sequences contain many epistatic interactions, and that many of these interactions increase affinity. Our approach involves first training an additive (PWM) model as a baseline, and identifying departures from that model as epistasis. In this comparison, a crucial step was to correct for the two issues of scale and measurement noise.

The first issue, identified by Fisher (Fisher, 1918) and also called unidimensional epistasis (Szendro et al., 2013), is the idea that an epistatic trait becomes additive upon a different parametrization (Sailer and Harms, 2017a). For instance, protein stability, which often determines fitness, is a nonlinear function of the folding free energy difference, which is expected to be roughly additive (Bloom et al., 2005; Bershtein et al., 2006; Jacquier et al., 2013; Gong et al., 2013; Serohijos and Shakhnovich, 2014; Bank et al., 2015; Sarkisyan et al., 2016). This leads to both a law of diminishing returns (Bank et al., 2015) and robustness to mutations when the protein is very stable (Bloom et al., 2005). To disentangle these potential artifacts, we defined our PWM on the binding free energy, which we expect to be additive in sequence content, and we checked that this parametrization was close to minimizing epistasis.

To tackle the second and perhaps more important issue of noise, especially in the context of deep mutational scans where many variants are tested (Araya et al., 2012), we developed a robust methodology based on Z-scores to identify epistatic interactions as significant outliers. This analysis showed that the variability in binding free energy consists of ~60% of additive effects, ~25%–35% of epistatic effects, and the rest of experimental noise, making the epistatic contribution to the phenotype substantial compared to that of single mutations. A large fraction of that epistasis was beneficial, in contrast with previous reports of mostly negative epistasis owing to the concavity of the scale (Bershtein et al., 2006; Schenk et al., 2013; Bank et al., 2015), which we here circumvent by directly considering the free energy.

Epistasis is key to understanding the predictability and reproducibility of evolutionary paths (Lässig et al., 2017; Kryazhimskiy et al., 2014). Previous studies have shown that much of the unexplained phenotypic variance could be explained by

second-order epistatic terms, although specific evolutionary trajectories may be sensitive to higher order epistatic terms (Sailer and Harms, 2017b; Poelwijk et al., 2017). Our results show how second-order epistasis could constrain the space of possible hyper-mutation trajectories during affinity maturation, with important consequences for antibody and vaccine design, as the importance of eliciting responses of antibodies that are not just strongly binding but also evolvable is being increasingly recognized (Wang et al., 2015). Targeting epistatic interactions may provide an alternative strategy for optimizing antibody affinity: among the 2 epistatic hotspots in CDR1H and the 11 in CDR3H that we identified $\left(\langle Z_{epi}^2\rangle^{\frac{1}{2}} > 3\right)$, 4 involved positions mutated in the super-optimized 4M5.3 antibody sequence, with a higher epistatic contribution than expected by chance. This is consistent with a previous study where an antibody with multiple conformations acquired mutations that stabilized the antibody structure, resulting in a single conformation (Wedemayer et al., 1997). We also identified 3 cases of beneficial sign epistasis, in which the double mutant was fit despite the single mutant being deleterious. For instance, the D108E mutations in 4M5.3 is deleterious by itself but is rescued beyond the wildtype value by the S101A mutation (Midelfort et al., 2004), which occurred first in the directed evolution process (Boder et al., 2000). We report 15 extreme cases of viable ($K_d < 10^{-6}$ M) double mutants whose single-mutant intermediates are nonviable, possibly blocking affinity maturation. However, our analysis of the volume and mutational flux of the region of low binding free energies in sequence space suggests that epistasis facilitates the evolution of high-affinity antibodies (Figures 2F and 2G). Therefore, we speculate that interactions with the non-mutated parts of the sequence and evolution of the antigen binding partner can either add further constraints or open up additional paths.

Antibodies pose unique questions about the evolvability of evolution (Wagner and Altenberg, 1996). What sort of sequence space would favor quick accessibility while maintaining a small number of viable sequences (Perelson and Oster, 1979)? A landscape could contain small, permeable, easily evolvable recognition spaces, or could contain large, hard to access, and robust sequences depending on the prevalent epistatic contributions (Carter et al., 2005). Such a bias could suggest that the tradeoff of an epistatic landscape would include fast initial evolution, followed by slow incremental evolution (Good and Desai, 2015). Our observations, deviating around a viable antibody variant, support a model where epistasis plays a lesser role in determining binding affinity than PWM terms, but could still have far ranging impacts. These impacts would include fast initial or slow long-term evolution, the blocking of paths to beneficial mutations, while paradoxically increasing the accessibility of antigen recognizing sequences.

Taken together, our results show the importance of taking into account epistasis when predicting antibody evolution and guiding vaccine design. We note that, while the yeast display system we studied is highly correlated to alternative measures of affinity (Gai and Wittrup, 2007), antibodies could behave differently under alternative environments. Specifically, a soluble antibody may experience different interactions with the environment and be subject to different constraints than an antibody expressed

on a cellular surface. Nevertheless, our systematic approach for identifying and quantifying epistasis, which controls for scale and noise, can be used by other investigators to analyze deep mutational scans of protein function in a wide variety of biological contexts.

STAR★METHODS

Detailed methods are provided in the online version of this paper and include the following:

- CONTACT FOR REAGENT AND RESOURCE SHARING
- METHOD DETAILS
  - Position Weight Matrix
  - Optimal Nonlinear Transformation of the Free Energy
  - Z-Scores
  - Null Model for Sign Epistasis
  - Epistatic Model
- QUANTIFICATION AND STATISTICAL ANALYSIS
- DATA AND SOFTWARE AVAILABILITY

SUPPLEMENTAL INFORMATION

Supplemental Information includes 16 figures and 2 tables and can be found with this article online at https://doi.org/10.1016/j.cels.2018.12.004.

AUTHOR CONTRIBUTIONS

Conceptualization, R.M.A., J.B.K., A.M.W., and T.M.; Methodology, R.M.A.; Software, R.M.A.; Validation, R.M.A.; Formal Analysis, R.M.A., A.M.W., and T.M.; Data Curation, R.M.A.; Writing – Original Draft, R.M.A., A.M.W., and T.M.; Writing – Review & Editing, J.B.K., A.M.W., and T.M.; Visualization, R.M.A.

DECLARATION OF INTERESTS

R.M.A. was employed by Novozymes at time of publication.

REFERENCES

Adams, R.M., Mora, T., Walczak, A.M., and Kinney, J.B. (2016). Measuring the sequence-affinity landscape of antibodies with massively parallel titration curves. Elife 5, e23156.

Andersen, M.S., Dahl, J., and Vandenberghe, L. (2013). CVXOPT: a python package for convex optimization, [1.1. version] 6, 54 cvxopt.org.

Anderson, D.W., McKeown, A.N., and Thornton, J.W. (2015). Intermolecular epistasis shaped the function and evolution of an ancient transcription factor and its DNA binding sites. Elife 4, 1–26.

Araya, C.L., Fowler, D.M., Chen, W., Muniez, I., Kelly, J.W., and Fields, S. (2012). A fundamental protein property, thermodynamic stability, revealed solely from large-scale measurements of protein function. Proc. Natl. Acad. Sci. USA 109, 16858–16863.

Asti, L., Uguzzoni, G., Marcatili, P., and Pagnani, A. (2016). Maximum-entropy models of sequenced immune repertoires predict antigen-antibody affinity. PLoS Comput. Biol. *12*, e1004870.

Bank, C., Hietpas, R.T., Jensen, J.D., and Bolon, D.N.A. (2015). A systematic survey of an intragenic epistatic landscape. Mol. Biol. Evol. *32*, 229–238.

Batista, F.D., and Neuberger, M.S. (1998). Affinity dependence of the B cell response to antigen: A threshold, a ceiling, and the importance of off-rate. Immunity *8*, 751–759.

Bershtein, S., Segal, M., Bekerman, R., Tokuriki, N., and Tawfik, D.S. (2006). Robustness-epistasis link shapes the fitness landscape of a randomly drifting protein. Nature *444*, 929–932.

Bloom, J.D., Gong, L.I., and Baltimore, D. (2010). Permissive secondary mutations enable the evolution of influenza oseltamivir resistance. Science *328*, 1272–1275.

Bloom, J.D., Labthavikul, S.T., Otey, C.R., and Arnold, F.H. (2006). Protein stability promotes evolvability. Proc. Natl. Acad. Sci. USA *103*, 5869–5874.

Bloom, J.D., Silberg, J.J., Wilke, C.O., Drummond, D.A., Adami, C., and Arnold, F.H. (2005). Thermodynamic prediction of protein neutrality. Proc. Natl. Acad. Sci. USA *102*, 606–611.

Boder, E.T., Midelfort, K.S., and Wittrup, K.D. (2000). Directed evolution of antibody fragments with monovalent femtomolar antigen-binding affinity. Proc. Natl. Acad. Sci. USA *97*, 10701–10705.

Boyer, S., Biswas, D., Kumar Soshee, A., Scaramozzino, N., Nizak, C., and Rivoire, O. (2016). Hierarchy and extremes in selections from pools of randomized proteins. Proc. Natl. Acad. Sci. USA *113*, 3482–3487.

Breen, M.S., Kemena, C., Vlasov, P.K., Notredame, C., and Kondrashov, F.A. (2012). Epistasis as the primary factor in molecular evolution. Nature *490*, 535–538.

Brenke, R., Hall, D.R., Chuang, G.-Y., Comeau, S.R., Bohnuud, T., Beglov, D., Schueler-Furman, O., Vajda, S., and Kozakov, D. (2012). Application of asymmetric statistical potentials to antibody-protein docking. Bioinformatics *28*, 2608–2614.

Carter, A.J.R., Hermisson, J., and Hansen, T.F. (2005). The role of epistatic gene interactions in the response to selection and the evolution of evolvability. Theor. Popul. Biol. *68*, 179–196.

Chou, H.-H., Chiu, H.-C., Delaney, N.F., Segrè, D., and Marx, C.J. (2011). Diminishing returns epistasis among beneficial mutations decelerates adaptation. Science *332*, 1190–1192.

Cobey, S., and Wilson, P. (2015). The evolution within us. Philos. Trans. R. Soc. Lond. B Biol. Sci. *370*.

Corti, D., and Lanzavecchia, A. (2013). Broadly neutralizing antiviral antibodies. Annu. Rev. Immunol. *31*, 705–742.

de Visser, J.A.G.M., and Krug, J. (2014). Empirical fitness landscapes and the predictability of evolution. Nat. Rev. Genet. *15*, 480–490.

Eisen, H.N., and Siskind, G.W. (1964). Variations in affinities of antibodies during the immune response. Biochemistry *3*, 996–1008.

Esmaielbeiki, R., Krawczyk, K., Knapp, B., Nebel, J.C., and Deane, C.M. (2016). Progress and challenges in predicting protein interfaces. Brief. Bioinform. *17*, 117–131.

Fisher, R. (1918). The correlation between relatives on the supposition of Mendelian inheritance. Trans. R. Soc. Edinb. *52*, 399–433.

Foote, J., and Eisen, H.N. (1995). Kinetic and affinity limits on antibodies produced during immune responses. Proc. Natl. Acad. Sci. USA *92*, 1254–1256.

Fowler, D.M., and Fields, S. (2014). Deep mutational scanning: a new style of protein science. Nat. Methods *11*, 801–807.

Gai, S.A., and Wittrup, K.D. (2007). Yeast surface display for protein engineering and characterization. Curr. Opin. Struct. Biol. *17*, 467–473.

George, J.T., Kessler, D.A., and Levine, H. (2017). Effects of thymic selection on T cell recognition of foreign and tumor antigenic peptides. Proc. Natl. Acad. Sci. USA *114*, E7875–E7881.

Gong, L.I., Suchard, M.A., and Bloom, J.D. (2013). Stability-mediated epistasis constrains the evolution of an influenza protein. Elife *2*, 1–19.

Good, B.H., and Desai, M.M. (2015). The impact of macroscopic epistasis on long-term evolutionary dynamics. Genetics *199*, 177–190.

Jacquier, H., Birgy, A., Le Nagard, H., Mechulam, Y., Schmitt, E., Glodt, J., Bercot, B., Petit, E., Poulain, J., Barnaud, G., et al. (2013). Capturing the mutational landscape of the beta-lactamase TEM-1. Proc. Natl. Acad. Sci. USA *110*, 13067–13072.

Kepler, T., Liao, H.-X., Alam, S.M., Bhaskarabhatla, R., Zhang, R., Yandava, C., Stewart, S., Anasti, K., Kelsoe, G., Parks, R., et al. (2014). Immunoglobulin gene insertions and deletions in the affinity maturation of HIV-1 broadly reactive neutralizing antibodies. Cell Host Microbe *16*, 304–313.

Koenig, P., Lee, C.V., Sanowar, S., Wu, P., Stinson, J., Harris, S.F., and Fuh, G. (2015). Deep sequencing-guided design of a high affinity dual specificity antibody to target two angiogenic factors in neovascular age-related macular degeneration. J. Biol. Chem. *290*, 21773–21786.

Kryazhimskiy, S., Rice, D.P., Jerison, E.R., and Desai, M.M. (2014). Microbial evolution. Global epistasis makes adaptation predictable Despite sequence-level stochasticity. Science *344*, 1519–1522.

Lässig, M., Mustonen, V., and Walczak, A.M. (2017). Predicting evolution. Nat. Ecol. Evol. *1*, 77.

Łuksza, M., Riaz, N., Makarov, V., Balachandran, V.P., Hellmann, M.D., Solovyov, A., Rizvi, N.A., Merghoub, T., Levine, A.J., Chan, T.A., et al. (2017). A neoantigen fitness model predicts tumour response to checkpoint blockade immunotherapy. Nature *551*, 517–520.

Marcou, Q., Mora, T., and Walczak, A.M. (2018). High-throughput immune repertoire analysis with IGoR. Nat. Commun. *9*, 561.

McLaughlin, R.N., Jr., Poelwijk, F.J., Raman, A., Gosal, W.S., and Ranganathan, R. (2012). The spatial architecture of protein function and adaptation. Nature *491*, 138–142.

Melamed, D., Young, D.L., Gamble, C.E., Miller, C.R., and Fields, S. (2013). Deep mutational scanning of an RRM domain of the Saccharomyces cerevisiae poly(A)-binding protein. RNA *19*, 1537–1551.

Midelfort, K.S., Hernandez, H.H., Lippow, S.M., Tidor, B., Drennan, C.L., and Wittrup, K.D. (2004). Substantial energetic improvement with minimal structural perturbation in a high affinity mutant antibody. J. Mol. Biol. *343*, 685–701.

Mora, T., Walczak, A.M., Bialek, W., and Callan, C.G. (2010). Maximum entropy models for antibody diversity. Proc. Natl. Acad. Sci. USA *107*, 5405–5410.

Morcos, F., Pagnani, A., Lunt, B., Bertolino, A., Marks, D.S., Sander, C., Zecchina, R., Onuchic, J.N., Hwa, T., and Weigt, M. (2011). Direct-coupling analysis of residue coevolution captures native contacts across many protein families. Proc. Natl. Acad. Sci. USA *108*, E1293–E1301.

Olson, C.A., Wu, N., and Sun, R. (2014). A comprehensive biophysical description of pairwise epistasis throughout an entire protein domain. Curr. Biol. *24*, 2643–2651.

Paixão, T., and Barton, N.H. (2016). The effect of gene interactions on the long-term response to selection. Proc. Natl. Acad. Sci. USA *113*, 4422–4427.

Park, T., and Casella, G. (2008). The Bayesian Lasso. J. Am. Stat. Assoc. *103*, 681–686.

Perelson, A.S., and Oster, G.F. (1979). Theoretical studies of clonal selection: minimal antibody repertoire size and reliability of self-non-self discrimination. J. Theor. Biol. *81*, 645–670.

Phillips, P.C. (2008). Epistasis - the essential role of gene interactions in the structure and evolution of genetic systems. Nat. Rev. Genet. *9*, 855–867.

Podgornaia, A.I., and Laub, M.T. (2015). Pervasive degeneracy and epistasis in a protein-protein interface. Science *347*, 673–677.

Poelwijk, F.J., Kiviet, D.J., Weinreich, D.M., and Tans, S.J. (2007). Empirical fitness landscapes reveal accessible evolutionary paths. Nature *445*, 383–386.

Poelwijk, F.J., Socolich, M., and Ranganathan, R. (2017). Learning the pattern of epistasis linking genotype and phenotype in a protein. bioRxiv, 213835.

Poelwijk, F.J., Tănase-Nicola, S., Kiviet, D.J., and Tans, S.J. (2011). Reciprocal sign epistasis is a necessary condition for multi-peaked fitness landscapes. J. Theor. Biol. *272*, 141–144.

Romero, P.A., Krause, A., and Arnold, F.H. (2013). Navigating the protein fitness landscape with Gaussian processes. Proc. Natl. Acad. Sci. USA *110*, E193–E201.

Roost, H.P., Bachmann, M.F., Haag, A., Kalinke, U., Pliska, V., Hengartner, H., and Zinkernagel, R.M. (1995). Early high-affinity neutralizing anti-viral IgG responses without further overall improvements of affinity. Proc. Natl. Acad. Sci. USA *92*, 1257–1261.

Sailer, Z.R., and Harms, M.J. (2017a). Detecting high-order epistasis in nonlinear genotype-phenotype maps. Genetics *205*, 1079–1088.

Sailer, Z.R., and Harms, M.J. (2017b). High-order epistasis shapes evolutionary trajectories. PLoS Comput. Biol. *13*, e1005541.

Sarkisyan, K.S., Bolotin, D.A., Meer, M.V., Usmanova, D.R., Mishin, A.S., Sharonov, G.V., Ivankov, D.N., Bozhanova, N.G., Baranov, M.S., Soylemez, O., et al. (2016). Local fitness landscape of the green fluorescent protein. Nature *533*, 397–401.

Schenk, M.F., Szendro, I.G., Salverda, M.L.M., Krug, J., De Visser, J.A.G.M., and Visser, J.A.G.M.D. (2013). Patterns of epistasis between beneficial mutations in an antibiotic resistance gene. Mol. Biol. Evol. *30*, 1779–1787.

Serohijos, A.W., and Shakhnovich, E.I. (2014). Merging molecular mechanism and evolution: theory and computation at the interface of biophysics and evolutionary population genetics. Curr. Opin. Struct. Biol. *26*, 84–91.

Szendro, I.G., Schenk, M.F., Franke, J., Krug, J., and De Visser, J.A.G.M. (2013). Quantitative analyses of empirical fitness landscapes. J. Stat. Mech. *2013*, https://doi.org/10.1088/1742-5468/2013/01/P01005.

VanAntwerp, J.J., and Wittrup, K.D. (2000). Fine affinity discrimination by yeast surface display and flow cytometry. Biotechnol. Prog. *16*, 31–37.

Vodnik, M., Zager, U., Strukelj, B., and Lunder, M. (2011). Phage display: selecting straws instead of a needle from a haystack. Molecules *16*, 790–817.

Voet, D., and Voet, J.G. (2011). Biochemistry, *4*, Fourth Edition (John Wiley& Sons Inc), pp. 68–69.

Wagner, G.P., and Altenberg, L. (1996). Perspective: complex adaptations and the evolution of evolvability. Evolution *50*, 967–976.

Wang, S., Mata-Fink, J., Kriegsman, B., Hanson, M., Irvine, D.J., Eisen, H.N., Burton, D.R., Wittrup, K.D., Kardar, M., and Chakraborty, A.K. (2015). Manipulating the selection forces during affinity maturation to generate cross-reactive HIV antibodies. Cell *160*, 785–797.

Wedemayer, G.J., Patten, P.A., Wang, L.H., Schultz, P.G., and Stevens, R.C. (1997). Structural insights into the evolution of an antibody combining site. Science *276*, 1665–1669.

Weinreich, D.M., Delaney, N.F., DePristo, M.A., and Hartl, D.L. (2006). Darwinian evolution can follow only very few mutational paths to fitter proteins. Science *312*, 111–114.

Weinreich, D.M., Watson, R.A., Chao, L., and Harrison, R. (2005). Perspective:sign epistasis and genetic constraint on evolutionary trajectories. Evolution *59*, 1165–1174.

Wells, J.A. (1990). Additivity of mutational effects in proteins. Biochemistry *29*, 8509–8517.

Zhang, X., Perica, T., and Teichmann, S.A. (2013). Evolution of protein structures and interactions from the perspective of residue contact networks. Curr. Opin. Struct. Biol. *23*, 954–963.

STAR★METHODS

CONTACT FOR REAGENT AND RESOURCE SHARING

Further information and requests for resources and reagents should be directed to and will be fulfilled by the Lead Contact, Thierry Mora (tmora@lps.ens.fr).

METHOD DETAILS

Position Weight Matrix

The amino-acid sequence of the 10 amino acid stretches of the CDR1H or CDR3H domains are denoted by $\mathbf{s} = (s_1,\ldots,s_{10})$. The corresponding 30-long nucleotide sequences are denoted by $\mathbf{v}$. The binding free energy $F(\mathbf{s})$ of an amino-acid variant is obtained as the mean over 3 replicate experiments, and over all its synonymous variants:

Values of Kd as Measured by Tite-Seq for Variants of the 4-4-20 Fluorescein-Binding Antibody (RRID: Addgene_41845) (Adams et al., 2016) can be found at https://github.com/jbkinney/16_titeseq.

The scripts used for the analyses presented here are available at https://github.com/rhys-m-adams/epistasis_4_4_20.

$$F(\mathbf{s}) = \frac{1}{N(\mathbf{s})} \sum_a \sum_{\mathbf{v} \in S_a(\mathbf{s})} \ln(K_d(\mathbf{v},a)/c_0), \tag{Equation 3}$$

where $S_a(\mathbf{s})$ is the set of measured nucleotide sequences that translate to $\mathbf{s}$ in replicate a, and $N(\mathbf{s}) = \sum_a |S_a(\mathbf{s})|$ is a normalization constant.

The elements of the PWM are defined as $h_i(q) = F(\mathbf{s}^{(i,q)}) - F_{WT}$, where $\mathbf{s}^{(i,q)}$ is the single mutant mutated at position i to residue q, and $h_i(q) = 0$ when q is the wild-type residue at position i.

Optimal Nonlinear Transformation of the Free Energy

To test whether transforming F through a nonlinear function $E(F)$ before learning the PWM could improve its predictive power, we defined the nonlinear additive model:

$$F(\mathbf{s}) \approx f[E_{PWM}(\mathbf{s})], \quad E_{PWM}(\mathbf{s}) = E_{WT} + \sum_i \tilde{h}_i(s_i), \tag{Equation 4}$$

where $f = E^{-1}$ is the inverse function of E, $\tilde{h}_i(q) = E(\mathbf{s}^{(i,q)}) - E_{WT}$, and $E(\mathbf{s})$ is evaluated similarly to Equation 3: $E(\mathbf{s}) = (1/N(\mathbf{s})) \sum_a \sum_{\mathbf{v} \in S_a(\mathbf{s})} E[\ln(K_d(\mathbf{v})/c_0)]$.

To find the transformation E that gives the highest explained variance while avoiding overfitting, we aimed to minimize the following objective function:

$$O[E] = \sum_{\mathbf{s}} [E_{PWM}(\mathbf{s}) - E(\mathbf{s})]^2 + \alpha \int dF |E''(F)|^2, \tag{Equation 5}$$

where the sum in $\mathbf{s}$ runs over double and triple mutants, and α is a tunable parameter.

Numerically, we parametrize the function $E(F)$ as piecewise linear: $E(F) = E_i \times (F_{i+1} - F)/\delta F + E_{i+1} \times (F - F_i)\delta F$ for $F_i \leq F \leq F_{i+1}$, where F_i are equally spaced grid points along F, $\delta F = F_{i+1} - F_i$, and E_i the value of E at these points. The smoothing penalty is approximated by a sum over the squared discretized second derivative:

$$\int df |E''(F)|^2 \approx \sum_u (E_{i+1} + E_{i-1} - 2E_i)^2 / \delta F^3.$$

We minimize $O[E] \approx O[E_1, \leftrightarrows, E_N]$ as a quadratic function of its arguments (E_i), while imposing boundary constraints on the PWM prediction and the requirement that E is a increasing function of F (i.e. $E_{i+1} > E_i$), using the python package cvxopt (Andersen et al., 2013).

The hyper-parameter α is evaluated by maximizing the generalized cross-validation of the coefficient of determination

$$R^2 = 1 - \left\langle \frac{\sum_{\mathbf{s} \in S} \left[E_{PWM}^{\backslash S}(\mathbf{s}) - E^{\backslash S}(\mathbf{s})\right]^2}{Var_{\mathbf{s} \in S}[E^{\backslash S}(\mathbf{s})]} \right\rangle_S, \tag{Equation 6}$$

where $E^{\backslash S}$ and $E_{PWM}^{\backslash S}$ are learned through optimizing Equation 5, but after removing from the dataset a subset S of the multiple mutants comprising one tenth of the total. The average is over ten nonoverlapping subsets S.

This method was first tested on simulated data. Each PWM element $\tilde{h}_i(q)$ was drawn from a normal distribution of zero mean and variance 1, and then $E_{PWM}(\mathbf{s})$ was computed for each of the antibody sequences present in our data. Our simulated "measurement" was defined as a function of a noisy realization of $E = E_{PWM} + \varepsilon$ (where ε is some Gaussian noise) in four different ways: linear $F=E$,

exponential $F=\exp(E)$, high-frequency $F=2E+\sin(2E)$, and logistic $F=1/[1+\exp(-E)]$. ε was drawn from a centered normal distribution with 1/2 the standard deviation of E_{PWM}. F was then truncated to the 200th lowest and 200th highest values, to mimic the boundary cutoff in our measurements. Comparing our original E_{PWM} to our fit $\hat{E}$ shows that our method is able to infer the true PWM model and a smooth nonlinearity from noisy data (Figure S5).

We then applied the method to the experimental data. The cross-validation R^2 is represented as a function of the smoothing parameter α in Figure S6A, and the corresponding optimal function $E(F)$ in Figure S6B. The comparison between measurement and the PWM model is shown in Figure S6C.

Z-Scores

We used synonymous mutants to estimate our measurement error. The mean free energy of a nucleotide sequence is defined as the mean over replicate measurements: $F(\mathbf{v}) = \langle \ln(K_d(\mathbf{v},a)) \rangle_a$, and the standard error $\sigma(\mathbf{v})$ is defined accordingly as the pooled error over replicates. Antibodies with K_d or single mutant PWM contributions having median values at the boundary values of $10^{-9.5}$ or 10^{-5} were excluded from the analysis since these values artificially cluster at the boundary, leading to underestimates of error.

The error Z-score was calculated between pairs of nucleotide sequences with the same amino acid translation: $Z_{error}(\mathbf{v}, \mathbf{v}') = (F(\mathbf{v}) - F(\mathbf{v}'))/\sqrt{\sigma(\mathbf{v})^2 + \sigma(\mathbf{v}')^2}$.

Epistatic Z-scores were estimated by calculating the measurement error over both replicates and synonymous variants, as in Equation 3:

$$\sigma^2(\mathbf{s}) = \frac{\sum_a \sum_{\mathbf{v} \in S_a(\mathbf{s})} [\ln(K_d(\mathbf{v},a)/c_0) - F(\mathbf{s})]^2}{N(\mathbf{s})(N(\mathbf{s}) - 1)} \qquad \text{(Equation 7)}$$

and the pooled standard error for a PWM prediction, calculated as the sum of measurement errors from single mutations:

$$\sigma^2_{PWM}(\mathbf{s}) = \sum_i \sigma^2_i(s_i), \qquad \text{(Equation 8)}$$

where $\sigma_i(q) = \sigma(\mathbf{s}^{(i,q)})$, and $\sigma_i(q) = 0$ when q is the wildtype residue at i. The epistatic Z-score is defined as:

$$Z_{epi}(\mathbf{s}) = \frac{F_{PWM}(\mathbf{s}) - F(\mathbf{s})}{\sqrt{\sigma^2(\mathbf{s}) + \sigma^2_{PWM}(\mathbf{s})}}. \qquad \text{(Equation 9)}$$

Null Model for Sign Epistasis

To calculate p-values for sign epistasis, we used the following null model for sets of four Z-scores satisfying $Z_A + Z_{B|A} = Z_B + Z_{A|B}$. Calling $x_1 = Z_A, x_2 = Z_{B|A}, x_3 = -Z_{A|B}, x_4 = -Z_A$, the condition becomes that each x_i has zero mean and variance one, with the constraint $\sum_{i=1}^4 x_i = 0$. The distribution with maximum entropy satisfying these requirements is a centered multi-variate Gaussian uniquely defined by its covariance matrix $\langle x_i^2 \rangle = 1$ and $\langle x_i x_j \rangle = -1/3$ for $i \neq j$. The p-value for sign epistasis, $Z_A > 1.65$ and $Z_{A|B} < 1.65$, was estimated by Monte Carlo sampling under a Gaussian distribution as
$$\begin{matrix} \Pr(x_1>1.65 \& x_2>1.65) + \\ \Pr(x_3>1.65 \& x_4>1.65) - \\ \Pr(x_1>1.65 \& x_2< -1.65 \& x_3>1.65 \& x_4< -1.65) \\ = 5.6 \cdot 10^{-4} \end{matrix}$$
, and the

probability for reciprocal sign epistasis as

$\Pr(x_1>1.65 \& x_2< -1.65 \& x_3>1.65 \& x_4< -1.65) = 9.8 \cdot 10^{-5}$. The threshold of 1.65, in contrast to the previous threshold of 1.64, was determined by applying the Benjamin-Hochberg method for limiting false discovery to 0.05.

Epistatic Model

The epistatic terms of the pairwise model were made to depend on the biochemical categories of the interacting residues, $J_{ij}(s_i,s_j) = \tilde{J}_{ij}(b(s_i),b(s_j))$, with $b(s)=$nonpolar for $s=$AFGILMPVW, $b(s)=$polar for $s=$CNQSTY, $b(s)=$acidic for $s=$DE, and $b(s)=$basic for $s=$HKR. A fifth category was added to correspond to the wildtype residue, so that $\tilde{J}_{ij}(\text{wildtype},b) = \tilde{J}_{ij}(b,\text{wildtype}) = 0$. The model was trained by minimizing the mean squared error with a regularization penalty over all matrices $\tilde{J}_{ij}(b,b')$:

$$\sum_{\mathbf{s}} \left[F(\mathbf{s}) - F_{pairwise}\left(\mathbf{s}, \tilde{J}\right) \right]^2 + \lambda \sum_{ijbb'} |\tilde{J}_{ij}(b,b')|. \qquad \text{(Equation 10)}$$

The Lasso penalty λ was learned by 10-fold cross-validation, and energy terms found in less than 2 sequences were excluded from the fit. Posterior values for $\tilde{J}$ terms were calculated using Bayesian Lasso (Park and Casella, 2008).

The volume and mutational flux were defined as:

$$V(B) = \sum_{\mathbf{s}} \Theta(B - K_d(\mathbf{s})) \qquad \text{(Equation 11)}$$

$$A(B) = \sum_{\mathbf{s}} \Theta(B - K_d(\mathbf{s})) \frac{1}{19\ell} \sum_{\mathbf{s}' \mid d(\mathbf{s},\mathbf{s}')=1} \Theta(K_d(\mathbf{s}') - B), \qquad \text{(Equation 12)}$$

where $\tau(x)$ is the Heaviside function, i.e. $\tau(x)=1$ if $x \geq 0$ and 0 otherwise; $d(\mathbf{s},\mathbf{s}')$ is the Hamming distance between two sequences; and $\ell=10$ is the sequence length. The normalization $19 \times \ell$ corresponds to the number of mutants $\mathbf{s}'$ at Hamming distance 1 from $\mathbf{s}$. The sums over $\mathbf{s}$ in Equations 11 and 12 have 20^{10} elements and are computationally intractable. To overcome this, we approximated the sum using a mixture of Monte-Carlo and complete enumeration, depending on the distance of $\mathbf{s}$ from the wildtype. Calling C_d the set of sequences $\mathbf{s}$ at Hamming distance d from wildtype, we used:

$$\sum_{\mathbf{s}} g(\mathbf{s}) \approx \sum_{d=0}^{l} \frac{|C_d|}{|\tilde{C}_d|} \sum_{s \in \tilde{C}_d} g(\mathbf{s}) \qquad \text{(Equation 13)}$$

where $g(\mathbf{s})$ is a function of $\mathbf{s}$ to be summed such as in V or A in Equations 11 and 12, and $\tilde{C}_d$ is a random subset of C_d of size $\min(|C_d|,$

$P_d)$, with $P_d = \binom{l}{d} \times \left(\left\lfloor P / \binom{l}{d} \right\rfloor \right) + 1$, where P is the maximum number of sequences one is willing to sample completely at

each d to perform the estimation, and where $|C_d| = \binom{l}{d} 19^d$. For small d, when $|C_d| \leq P_d$, the enumeration is complete, while for

large d and $|C_d| > P_d$, the sum is estimated from a uniformly distributed Monte Carlo sample of C_d.

QUANTIFICATION AND STATISTICAL ANALYSIS

All analyses were performed using Python 3.6. Standard statistical tests such as F-test for model comparison (Figures 1C and 1D), Kolmogorov-Smirnov test for normality (Figure 2B), Levene's test for equal variance (Figure 2B), Mann-Whitney test for equal epistatic contributions by residue position (Figure 2C), and Binomial test for enrichment of sign epistasis (Method Details: Null model for sign epistasis) were performed using the scipy.stats module. Bayesian Lasso (Figures 2D and 2E), cross-validation (Figures 2D and 2E), and jackknifing (Figures 2F and 2G) estimates of probabilities are described in Method Details, were implemented using Python 3.6, and can be found at https://github.com/rhys-m-adams/epistasis_4_4_20.

DATA AND SOFTWARE AVAILABILITY

The scripts used for the analyses presented here are available at https://github.com/rhys-m-adams/epistasis_4_4_20. The original data is stored in BioProject PRJNA344711, and its original analysis including K_d measurements can be found at https://github.com/jbkinney/16_titeseq.